

ADDITIVE FABRICATION OF 3D STRUCTURES BY HOLOGRAPHIC LITHOGRAPHY

Maxim Shusteff^{1,2*}, Robert M. Panas¹, Johannes Henriksson¹, Brett E. Kelly^{1,3},
Allison E. M. Browar^{1,4}, Nicholas X. Fang⁵, Christopher M. Spadaccini¹

¹*Lawrence Livermore National Laboratory, Livermore, CA 94550, USA,*

²*Dept. of Electrical Engineering and Computer Science, Massachusetts Institute of Technology,
Cambridge, MA 02139, USA*

³*Dept. of Mechanical Engineering, University of California, Berkeley, CA 94720, USA*

⁴*Department of Mechanical Engineering, University of Rochester, Rochester, NY 14627, USA*

⁵*Dept. of Mechanical Engineering, Massachusetts Institute of Technology, Cambridge, MA
02139, USA*

Corresponding author: Email: shusteff1@llnl.gov Tel.: +1-925-423-0733

Abstract

As additive manufacturing (AM) technologies advance and mature, the geometric constraints imposed by fabricating 2D planar layers become increasingly important to overcome. In the realm of light-driven AM fabrication, holography provides a promising avenue toward true 3D structures. Being capable of recording and reconstructing 3D information, holographic shaping of the light field can enable direct 3D fabrication in photopolymer resins. We have conceptualized, designed, and built a prototype holographic additive micromanufacturing system, incorporating a liquid-crystal-on-silicon (LCoS) spatial light modulator (SLM) to redirect light energy at the build volume by spatial control of the phase distribution. Here we report the system design, design parameter trade-offs relevant for producing 3D structures, and initial fabrication results.

Introduction

The conceptual framework of additive manufacturing (AM) is to make things in a bottom-up fashion, adding material to create a part or structure, rather than carving, machining, or cutting it away from a larger piece. [1] This approach has held out the promise of efficient, rapid, and flexible fabrication of many types of three-dimensional (3D) structures and architected materials, with the important benefits of reducing wasted material, expanding geometric flexibility, and allowing the fabrication of engineered materials. Indeed, many of these advantages are beginning to be explored and demonstrated, including engineered biomimetic structures [2, 3], and engineered metamaterials with extraordinary properties [4]–[7].

Every AM process can be considered to employ some “unit operation” which is repeated to build up a complex part. Considering the range of such unit operations, the most serial, lowest-throughput processes deposit or photopolymerize one volume element (or “voxel”) at a time, which can be referred to as “zero-dimensional-plus” or 0D+ fabrication (a voxel is a zero-dimensional element). This includes technologies such as conventional stereolithography (SL) [8, 9], metal powder-bed-based laser fusing systems [10] as well as the familiar fused deposition

modeling (FDM) method used by desktop 3D printers writing with extruded plastic. Although advanced 0D+ technologies like direct laser writing (DLW) [11] and direct ink writing (DIW) [12] offer the capability of writing arbitrary paths in 3D space, rather than being constrained to planar layers, these are still fundamentally serial processes, and inherently low-throughput. Technologies based on layer-at-once rather than voxel-at-once unit operations yield approaches that can be called “2D+”. One example is projection micro-stereolithography (PμSL) [13], in which an LED-illuminated microdisplay is used to project full 2D images to cross-link layers of photopolymer resin. This enables significant gains in build speed. Nevertheless, this and other 2D+ approaches still carry with them some limitations inherent to building 2D layers. For instance, some geometries such as overhangs are difficult or impossible to reproduce accurately.

AM processes with “volume-at-once” unit operations, to produce complex 3D structures in a single step have remained a major challenge. Some promising recent reports include the use of multi-beam interference to generate periodic 3D lattice structures [14]–[17], and to modulate such lattices with aperiodic features [18, 19]. However, volume-at-once fabrication of aperiodic geometries that overcome the geometric limitations of these lattices has not previously been demonstrated. Additionally, in 2D+ layer-by-layer approaches, resin surface settling and planarization time is one of the slowest time-limiting steps, so overcoming this bottleneck is highly desirable. Ideally, this would be accomplished by fabricating away from the resin surface, within the bulk of the fluid. A secondary benefit of working within the bulk is avoiding oxygen concentration gradients associated with the fluid-air interface. Diffused oxygen plays an important role in photochemical kinetics, and proximity to a surface incurs additional complexity for properly controlling curing rates and geometry.

We are therefore interested in achieving an AM process capable of depositing or solidifying a complex volume as its unit operation, providing an additional leap forward in fabrication speed, and further reducing the limitations on the geometry of fabricated parts. In this work, we extend the polymer resin-based AM paradigm into the volume-at-once realm, providing the first demonstration of generating complex 3D structures in photopolymer as a unit operation.

The enabling technology is digital holography, a powerful paradigm for both recording and reconstructing 3D geometrical information. Using a diffractive element to phase-modulate a coherent laser beam, multiple sub-images of a holographically-shaped light field are directed such that they intersect within the resin volume. The light distribution is designed to deliver energy maxima to the desired regions of the resin that are to be cured. The part forms *in situ* in ~10 seconds, without requiring any support structure, nor layer-by-layer curing. Our initial results produce millimeter-scale parts with ~100 μm resolution. The results demonstrated here are suggestive of additional possibilities for this approach, and we discuss them at the conclusion of this manuscript.

System Configuration and Operation

A generalized light-directed AM system comprises four key subsystems, which are (1) the light source and beam conditioning, (2) pattern formation, (3) pattern projection/delivery, and (4) the photopolymer resin. While the parameter space for a holographic lithography system is

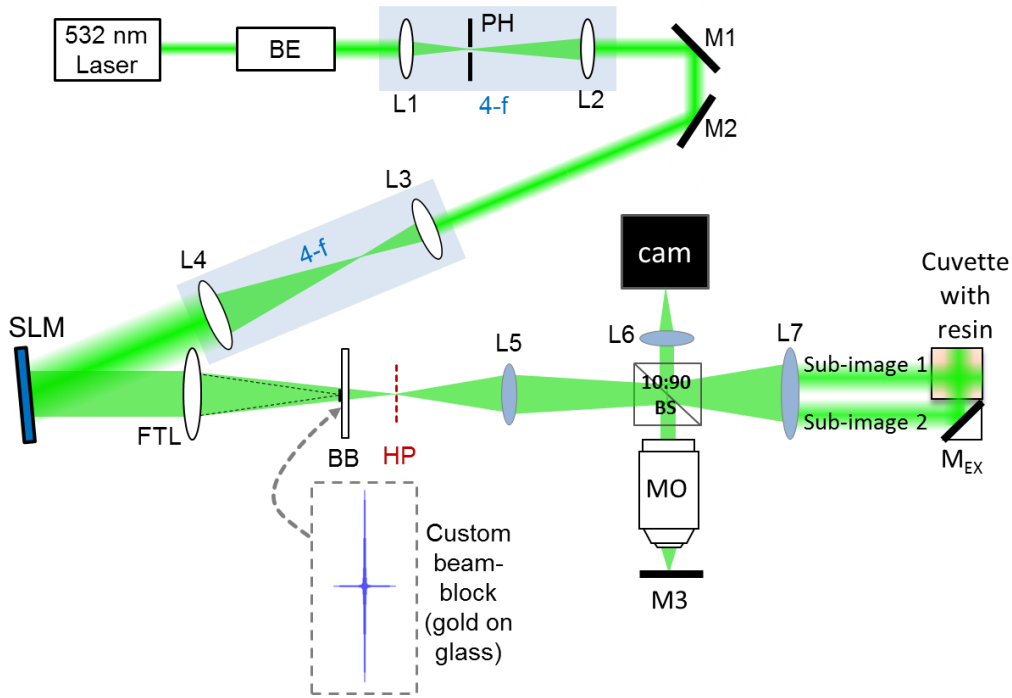


Figure 1: Optical configuration of the holographic 3D fabrication system. Lens pairs L1-L2 and L3-L4 are telescope pairs that size the beam correctly to impinge on the SLM, with the pinhole (PH) providing spatial filtering. The Fourier-transforming lens (FTL, $f=250$ mm) projects the phase hologram displayed on the SLM, forming the desired intensity distribution at the hologram plane (HP). This plane is displaced from the FTL natural focal plane (where the beam block BB is placed) by phase curvature added to the phase mask of the SLM, whereas undiffracted light is removed by the BB pattern. Lenses L5 and L7 are an image relay telescope pair, projecting the 3D intensity pattern into the resin with the help of exposure mirror M_{EX} . In a 3-beam configuration, a second mirror under the cuvette (out of plane) directs a third sub-image into the cuvette from a third orthogonal direction. The microscope objective MO and mirror M3 aid in monitoring image quality and exposure testing at reduced magnification when M3 is replaced by a sample.

very broad [20, 21], two key considerations drive the overall technology choices and system architecture in this work. The first is that holographic shaping of the light field requires a source with a high degree of spatial and temporal coherence, for useful diffraction and interference. This system is therefore designed around a narrow spectral linewidth single-mode (TEM_{00}) laser source. The second design consideration is that holographic beam shaping is most robust and straightforward with a phase-only spatial light modulator (SLM). With an appropriate phase pattern applied to this dynamic element the light field is Fourier-transformed by the projection optics to produce the desired intensity distribution at the build volume, photocuring the resin into the desired pattern.

In the current implementation, the 3D intensity pattern is produced by folding sub-regions of the projected light field using 45-degree mirrors placed in proximity to the final build volume. These sub-regions enter the build volume at right angles to one another, effectively forming intersecting beams, each of which carries an arbitrary image pattern. The intersection of

these patterns results in a complex 3D pattern with controllable areas of high intensity, and with appropriately chosen exposure parameters the 3D structure is formed. This approach is one of several possible paths to obtaining complex 3D light patterns, and we address alternative configurations in the Discussion section. The overall optical layout is shown in Fig. 1, and key subsystems are described in greater detail below.

Laser Source and Beam Conditioning

The holographic principle allows the recording and reconstruction of 3D geometric information by capturing the amplitude *and phase* information contained within a light field. Holographic reconstruction requires the use of light waves capable of interference, which implies a single-frequency laser for temporal coherence. In addition, the light delivered to the SLM must ideally consist of flat phase-front plane waves, which implies spatial coherence. In this work, we use a Coherent Verdi V-6 532 nm DPSS laser, specified by the manufacturer to have a linewidth of < 5 MHz (< 0.000005 nm, corresponding to a coherence length of > 50 m). The output beam is slightly expanded and spatially filtered through a $25\ \mu\text{m}$ pinhole, to improve the circularity and spatial coherence, then expanded again such that it reaches the SLM as a Gaussian beam with a $1/e^2$ diameter of approximately 20 mm. This is sized to approximately match the SLM diagonal, providing a balance in the trade-off between illumination uniformity, and efficient use of laser energy.

It is worth noting that the laser's minimal coherence length requirement is much shorter than that of the Verdi DPSS laser in our system: it must only exceed the path length differences between any light paths in the system that must interfere. In our configuration, this is only ~ 1 cm. However, additional coherence improves the contrast of reconstructed intensity fields at the build volume, thus benefitting lithographic fidelity; this remains to be rigorously characterized.

Pattern Formation: Computer-Generated Holograms

The digital phase mask required to produce a desired intensity distribution at the build volume is referred to as a computer-generated hologram (CGH). To imprint the phase mask onto the incident laser light we employ a liquid-crystal-on-silicon (LCoS) pixelated phase-only SLM

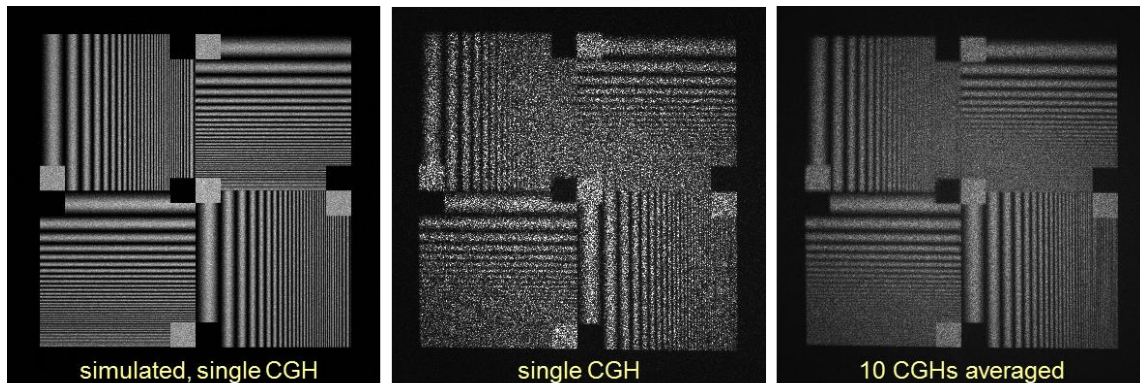


Figure 2: Holographic projection of a resolution test pattern, demonstrating the improved noise performance from averaging multiple CGHs generated to produce the same intensity pattern, initialized with a different random phase for each CGH. The simulated projection at left shows a Fourier transform of a single CGH in MATLAB, and the middle panel is the same CGH projected through our optical system and recorded with a CCD camera. The panel at right averages 10 separately recorded CGHs.

(Holoeye GmbH, PLUTO VIS). The use of a phase-only SLM for holographic light projection is well established, with various investigators working to calibrate [22], linearize [23], and otherwise characterize the LC behavior [24] for reliable operation. In the 1920×1080 pixel microdisplay used for this work, each 8μm square pixel imposes a phase delay between 0 and approximately 2.1π , controlled with 8-bit image data (256 gray levels), using a linear phase lookup table provided by the manufacturer.

The CGH is iteratively calculated by the well-known Gerchberg-Saxton (G-S) algorithm [25] to result in the desired light intensity distribution at the build volume. Many other methods for calculating phase holograms have been described [26]–[29], and some of these result in substantially higher-quality images, but these often impose much greater computational costs, or some may only be used with limited geometries. The simplicity and speed of the G-S approach, and in particular its generality when producing unconstrained and arbitrary image patterns, make it the most appropriate choice in this situation.

An ever-present consequence of using highly coherent illumination is speckle, arising from self-interference of the beam as it propagates through the optical system. This intensity variation is particularly problematic for lithography, since it directly affects the fidelity of pattern reconstruction. In SLM-based holography, the speckle noise is exacerbated by the digital noise arising from CGH calculation, as well as the discrete phase steps of the SLM pixels. However, it is straightforward to calculate multiple versions of a CGH that produce the same intensity pattern, by seeding the G-S algorithm with an initially random phase. Each of the resulting CGHs will then have different uncorrelated noise (and thus, speckle), and exposing them in rapid succession allows for an averaging effect that significantly improves the noise performance (estimated from statistical considerations to be a factor \sqrt{N} for N CGHs). The Holoeye PLUTO SLM used in this work is capable of cycling through CGHs at approximately 15 Hz, and each projected pattern uses $N = 10$ different CGHs for speckle/noise reduction (see Figure 2).

Eliminating Undiffracted Light

One of the most significant obstacles to the flexible and robust control of the light field in diffraction-based systems is eliminating interference from undiffracted light. Some fraction of the incident laser power reflects from the SLM without being modulated by the LC layer, generating an unwanted bright spot at the center of the build volume (with the intensity pattern that's the Fourier transform of the SLM rectangular aperture). Of the many approaches to mitigating and eliminating interference from this uncontrolled light [30]–[33], we concluded that incorporating a beam block at the Fourier plane of the hologram projection lens is the most robust implementation in this context. This approach is not pattern-dependent, nor does it require exhaustive SLM calibration and aberration compensation; once the beam block is aligned, additional adjustments are rarely necessary.

The shape of the beam block is designed to maximize its efficiency in rejecting undiffracted light, while allowing maximum transmission of the holographically-controlled light field. We fabricated custom glass flats with a gold metal film to block the spot, patterned in a “star” shape, matching the dimensions of the undiffracted spot (see inset, Fig. 1). Then, by adding a controlled phase curvature (Fresnel lens) to the CGH, which increases the effective focal length of the projection lens, the desired hologram itself is displaced away from the beam

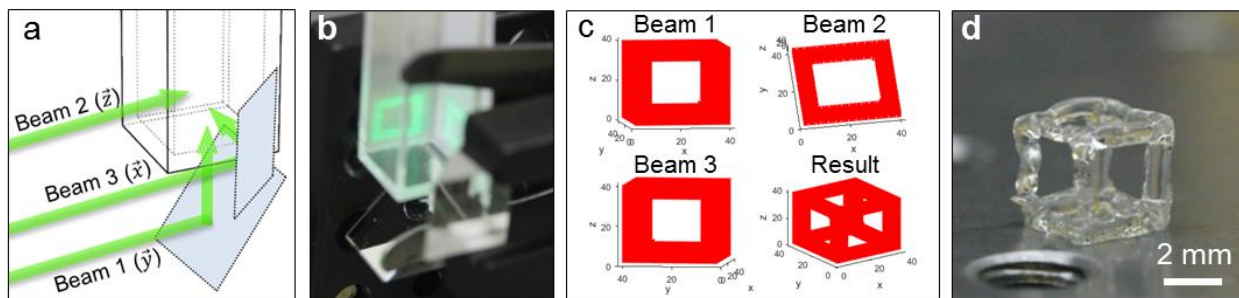


Figure 3: Single-exposure holographic fabrication of a 3D structure. (a) A representation of the incident beam geometry, with 45° mirrors reflecting two beams (which are subregions of the projected holographic field) along orthogonal directions to the original beam. (b) Photo of the cuvette before filling with resin, with paper screens at two sides for visualization of the projected pattern. (c) MATLAB point cloud representations of the propagating intensities for the three beams, and the region where they overlap in space. (d) The resulting part, after a single exposure of 12 s.

block plane, thereby allowing use of the full hologram space, with virtually no interference from undiffracted light.

Build Volume and Photopolymer

Since we are interested in 3D structure formation within the bulk of a liquid photopolymer, rather than in layers at a surface, this requires a resin formulation that is minimally absorptive. The resin used here is poly(ethylene glycol) diacrylate (PEGDA, MW=250) with 0.04% (w/w) Irgacure 784, which is a titanocene free-radical photoinitiator with its absorbance spectrum extending to the 532 nm wavelength of the laser source. At the same time, the use of intersecting patterned beams requires optical access from at least three sides of the build volume. Therefore, to hold the resin volume of approx. 1 mL, we use a fluorometer cell (Starna Cells, 3-G-10) with $10 \times 10 \times 45$ mm internal volume, and 1.25 mm thick polished glass sides and bottom. As with many resin-based systems, exposure doses vary depending on optical power density and geometry. With the 3-beam configuration, polymer parts were successfully produced using 12 s exposures at an estimated power of 30 mW/cm^2 incident onto the cuvette from each side, corresponding to an estimated volumetric cure dose of $\sim 45 \text{ mJ/mm}^3$.

Results and Discussion

Figure 3 summarizes the fabrication of a 3D cube structure using this holographic platform. Figure 4 on the next page shows several other fabricated geometries. We have chosen to fabricate millimeter-scale structures at this stage for simplicity of handling and geometric accessibility, but the part size and corresponding minimal feature scale can be readily adjusted by changing the magnification of the final projection optics. We intend to explore the resolution limits of this platform in future work.

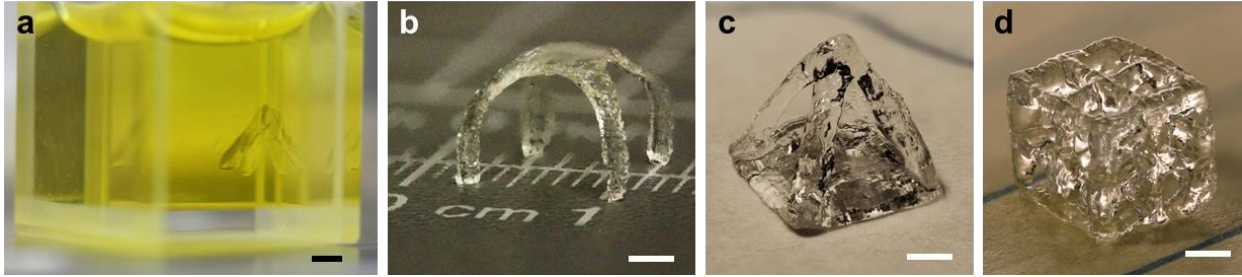


Figure 4: 3D structures fabricated with two-beam (a and b) and three-beam (c and d) exposures. (a) Shows the part *in situ* supported by the wall of the cuvette, however other parts form in the bulk volume, with no supporting structure. (b) This structure demonstrates the capability to produce structures with smoothly curving geometry without requiring layer-by-layer fabrication. Scale bars in all images are 2 mm.

As evident from Figures 3 and 4, the three intersecting light patterns behave much like collimated beams, though this is not technically accurate. Rather, their depth of focus (DOF) is large enough such that there is negligible variation in the pattern over its 10 mm propagation through the build volume. The intersection volumes of the three patterns are cured in the resulting 3D structure. Thus, in the present implementation, we are constrained to “extruded” geometries whose cross-section along any one axis does not vary with single-exposure structures. Several approaches for moving beyond this limitation are noted below.

The large DOF is a consequence of the SLM diffraction characteristics, as well as the final projection optics. These optics may be chosen with shorter focal lengths to reduce the effective system magnification, producing smaller-sized parts, and simultaneously increasing the numerical aperture (NA) at the build volume. This will improve axial resolution. However, this is fundamentally limited by the maximum diffraction angle available from the SLM pixels, as described by the diffraction grating equation $a(\sin \theta_d - \sin \theta_i) = n\lambda$ where a is the grating pitch, n is the diffracted order, and θ_i and θ_d are the incident and diffracted beam angle, respectively. For an SLM with 8 μm pixels diffracting 532 nm light, the angular spacing between diffracted orders is approximately 3.8° , corresponding to $\text{NA} \approx 0.07$ in air.

Whyte and Courtial [34] provide a useful analysis of how NA limitations affect the accessible spatial frequencies of a holographically reconstructed geometry. The result, in brief, is that the spatial frequency (i.e. intensity variation) of the light field along the direction of propagation (k_z) is necessarily very small for low-NA systems. We estimate that using this SLM, the maximum axial resolution is 0.25 mm at the HP and 0.5 mm at the cuvette due to the image magnification from lens pair L5 and L7 (see Fig. 1). However, this axial resolution is only attainable when lateral spatial frequency components in the pattern (k_x and k_y) are small, since these wave vectors in monochromatic light are related by $k_x^2 + k_y^2 + k_z^2 = k_0^2$ where $k_0 = 2\pi/\lambda$. Since the target intensity pattern is currently specified in a single plane, and the G-S algorithm is implemented for 2D fields, only the lateral spatial frequency components k_x and k_y are explicitly included in the calculation, and are privileged over any optimization of k_z .

The advantage of the approach described here is that the low spatial frequency in z can be compensated for with the higher spatial frequencies in x and y , by the folding of the light field, provided by the 45° mirrors. Taking advantage of this feature has already enabled the fabrication

of the structures shown here. Moreover, we expect that the “extruded” geometry limitation will be overcome, by incorporating 3D Gerchberg-Saxton calculations of the phase field, and building the “folding” capability into the iterative algorithm. This will allow the G-S algorithm to directly iterate on the 3D light field, providing further control on the image, and making more complex geometries routinely accessible with full control over all three spatial frequencies within the build volume.

Conclusion and Outlook

This work constitutes the first demonstration of direct fabrication of unsupported aperiodic 3D structures, using a “volume-at-once” unit operation for photopolymer curing, without requiring a layer-by-layer process. We anticipate that this paradigm in 3D fabrication will bring considerable advances in fabrication speed and geometric flexibility to the field of photopolymer-based AM. Additional geometric flexibility, as well as a larger overall build volume (or greater resolution in a small build volume), may be attained by using multiple SLMs illuminated by the same laser source, which project holographically interfering beams into the same resin volume.

Although the part quality achieved thus far is low, this is not an inherent limitation for this method. Additional speckle noise reduction by de-speckling techniques, in addition to optimization of curing parameters with adjustment of the intensity distribution in the three sub-images will enable high-quality part fabrication.

Acknowledgments

This work was performed under the auspices of the U.S. Department of Energy by Lawrence Livermore National Laboratory under Contract DE-AC52-07NA27344, with funding from the LLNL Laboratory Directed Research and Development (LDRD 14-SI-004) program. LLNL-CONF-697811

References

- [1] I. Gibson, D. Rosen, and B. Stucker, *Additive Manufacturing Technologies*. New York, NY: Springer New York, 2015.
- [2] G. Villar, A. D. Graham, and H. Bayley, “A Tissue-Like Printed Material,” *Science*, vol. 340, no. 6128, pp. 48–52, Apr. 2013.
- [3] H. N. Chia and B. M. Wu, “Recent advances in 3D printing of biomaterials,” *J. Biol. Eng.*, vol. 9, no. 1, Dec. 2015.
- [4] X. Zheng, H. Lee, T. H. Weisgraber, M. Shusteff, J. DeOtte, E. B. Duoss, J. D. Kuntz, M. M. Biener, Q. Ge, J. A. Jackson, S. O. Kucheyev, N. X. Fang, and C. M. Spadaccini, “Ultralight, ultrastiff mechanical metamaterials,” *Science*, vol. 344, no. 6190, pp. 1373–1377, Jun. 2014.
- [5] E. B. Duoss, T. H. Weisgraber, K. Hearon, C. Zhu, W. Small, T. R. Metz, J. J. Vericella, H. D. Barth, J. D. Kuntz, R. S. Maxwell, C. M. Spadaccini, and T. S. Wilson, “Three-Dimensional Printing of Elastomeric, Cellular Architectures with Negative Stiffness,” *Adv. Funct. Mater.*, vol. 24, no. 31, pp. 4905–4913, Aug. 2014.
- [6] T. Bückmann, M. Thiel, M. Kadic, R. Schittny, and M. Wegener, “An elasto-mechanical unfeleability cloak made of pentamode metamaterials,” *Nat. Commun.*, vol. 5, Jun. 2014.

- [7] C. Zhu, T. Liu, F. Qian, T. Y.-J. Han, E. B. Duoss, J. D. Kuntz, C. M. Spadaccini, M. A. Worsley, and Y. Li, “Supercapacitors Based on Three-Dimensional Hierarchical Graphene Aerogels with Periodic Macropores,” *Nano Lett.*, vol. 16, no. 6, pp. 3448–3456, Jun. 2016.
- [8] C. W. Hull, “United States Patent: 4575330 - Apparatus for production of three-dimensional objects by stereolithography,” 4575330, 11-Mar-1986.
- [9] P. J. Bártolo and I. Gibson, “History of Stereolithographic Processes,” in *Stereolithography*, P. J. Bártolo, Ed. Boston, MA: Springer US, 2011, pp. 37–56.
- [10] C. Kamath, B. El-dasher, G. F. Gallegos, W. E. King, and A. Sisto, “Density of additively-manufactured, 316L SS parts using laser powder-bed fusion at powers up to 400 W,” *Int. J. Adv. Manuf. Technol.*, vol. 74, no. 1–4, pp. 65–78, Sep. 2014.
- [11] J. B. Mueller, J. Fischer, F. Mayer, M. Kadic, and M. Wegener, “Polymerization Kinetics in Three-Dimensional Direct Laser Writing,” *Adv. Mater.*, vol. 26, no. 38, pp. 6566–6571, Oct. 2014.
- [12] D. B. Kolesky, R. L. Truby, A. S. Gladman, T. A. Busbee, K. A. Homan, and J. A. Lewis, “3D Bioprinting of Vascularized, Heterogeneous Cell-Laden Tissue Constructs,” *Adv. Mater.*, vol. 26, no. 19, pp. 3124–3130, May 2014.
- [13] X. Zheng, J. Deotte, M. P. Alonso, G. R. Farquar, T. H. Weisgraber, S. Gemberling, H. Lee, N. Fang, and C. M. Spadaccini, “Design and optimization of a light-emitting diode projection micro-stereolithography three-dimensional manufacturing system,” *Rev. Sci. Instrum.*, vol. 83, no. 12, p. 125001, Dec. 2012.
- [14] J. Xu, “Fabrication of photonic quasicrystals using holographic lithography method,” Hong Kong Univ. of Sci. And Tech. (Hong Kong), 2007.
- [15] T. A. Schaedler, A. J. Jacobsen, A. Torrents, A. E. Sorensen, J. Lian, J. R. Greer, L. Valdevit, and W. B. Carter, “Ultralight Metallic Microlattices,” *Science*, vol. 334, no. 6058, pp. 962–965, Nov. 2011.
- [16] K. Ohlinger, J. Lutkenhaus, B. Arigong, H. Zhang, and Y. Lin, “Spatially addressable design of gradient index structures through spatial light modulator based holographic lithography,” *J. Appl. Phys.*, vol. 114, no. 21, p. 213102, 2013.
- [17] H. Ning, J. H. Pikul, R. Zhang, X. Li, S. Xu, J. Wang, J. A. Rogers, W. P. King, and P. V. Braun, “Holographic patterning of high-performance on-chip 3D lithium-ion microbatteries,” *Proc. Natl. Acad. Sci.*, vol. 112, no. 21, pp. 6573–6578, May 2015.
- [18] M. C. Leibovici, G. M. Burrow, and T. K. Gaylord, “Pattern-integrated interference lithography: prospects for nano-and microelectronics,” *Opt. Express*, vol. 20, no. 21, pp. 23643–23652, 2012.
- [19] M. C. R. Leibovici and T. K. Gaylord, “Custom-modified three-dimensional periodic microstructures by pattern-integrated interference lithography,” *J. Opt. Soc. Am. A*, vol. 31, no. 7, p. 1515, Jul. 2014.
- [20] S. Zwick, T. Haist, M. Warber, and W. Osten, “Dynamic holography using pixelated light modulators,” *Appl. Opt.*, vol. 49, no. 25, p. F47, Sep. 2010.
- [21] T. Haist and W. Osten, “Holography using pixelated spatial light modulators—part 1: theory and basic considerations,” *J. MicroNanolithography MEMS MOEMS*, vol. 14, no. 4, p. 41310, Sep. 2015.
- [22] D. Engström, M. Persson, J. Bengtsson, and M. Goksör, “Calibration of spatial light modulators suffering from spatially varying phase response,” *Opt. Express*, vol. 21, no. 13, p. 16086, Jul. 2013.

- [23] F. J. Martínez, A. Márquez, S. Gallego, M. Ortuño, J. Francés, A. Beléndez, and I. Pascual, “Electrical dependencies of optical modulation capabilities in digitally addressed parallel aligned liquid crystal on silicon devices,” *Opt. Eng.*, vol. 53, no. 6, p. 67104, Jun. 2014.
- [24] A. Georgiou, J. Christmas, J. Moore, A. Jeziorska-Chapman, A. Davey, N. Collings, and W. A. Crossland, “Liquid crystal over silicon device characteristics for holographic projection of high-definition television images,” *Appl. Opt.*, vol. 47, no. 26, pp. 4793–4803, 2008.
- [25] R. W. Gerchberg and W. O. Saxton, “A Practical Algorithm for the Determination of Phase from Image and Diffraction Plane Pictures,” *Optik*, vol. 35, no. 2, pp. 227–246, 1972.
- [26] M. A. Seldowitz, J. P. Allebach, and D. W. Sweeney, “Synthesis of digital holograms by direct binary search,” *Appl. Opt.*, vol. 26, no. 14, pp. 2788–2798, 1987.
- [27] J. R. Fienup, “Phase retrieval algorithms: a comparison,” *Appl. Opt.*, vol. 21, no. 15, p. 2758, Aug. 1982.
- [28] R. Di Leonardo, F. Ianni, and G. Ruocco, “Computer generation of optimal holograms for optical trap arrays,” *Opt. Express*, vol. 15, no. 4, pp. 1913–1922, 2007.
- [29] A. Georgiou, J. Christmas, N. Collings, J. Moore, and W. A. Crossland, “Aspects of hologram calculation for video frames,” *J. Opt. Pure Appl. Opt.*, vol. 10, no. 3, p. 35302, Mar. 2008.
- [30] D. Palima and V. R. Daria, “Holographic projection of arbitrary light patterns with a suppressed zero-order beam,” *Appl. Opt.*, vol. 46, no. 20, pp. 4197–4201, 2007.
- [31] H. Zhang, J. Xie, J. Liu, and Y. Wang, “Elimination of a zero-order beam induced by a pixelated spatial light modulator for holographic projection,” *Appl. Opt.*, vol. 48, no. 30, pp. 5834–5841, 2009.
- [32] E. Ronzitti, M. Guillon, V. de Sars, and V. Emiliani, “LCoS nematic SLM characterization and modeling for diffraction efficiency optimization, zero and ghost orders suppression,” *Opt. Express*, vol. 20, no. 16, pp. 17843–17855, 2012.
- [33] J. Liang, S.-Y. Wu, F. K. Fatemi, and M. F. Becker, “Suppression of the zero-order diffracted beam from a pixelated spatial light modulator by phase compression,” *Appl. Opt.*, vol. 51, no. 16, pp. 3294–3304, 2012.
- [34] G. Whyte and J. Courtial, “Experimental demonstration of holographic three-dimensional light shaping using a Gerchberg–Saxton algorithm,” *New J. Phys.*, vol. 7, pp. 117–117, May 2005.